Check for updates

Fabrication of bio-based polyurethane nanofibers incorporated with a triclosan/cyclodextrin complex for antibacterial applications

Joo Hyung Lee,†[a] Sang Ho Park†[b] and Seong Hun Kim [ID] *[a]

A hybrid polyol consisting of a polycaprolactone diol/castor oil mixture was used to synthesize a biopolyurethane (BPU) that has a dendritic point but is soluble in organic solvents. The chemical structure of the obtained BPU was determined using Fourier transform infrared (FT-IR) spectroscopy and proton nuclear magnetic resonance spectroscopy. The mechanical properties of the electrospun BPU nanofiber were confirmed using a universal testing machine. To enhance the solubility of triclosan (TR), TR–cyclodextrin (CD) complexes were prepared. αCD, βCD, and γCD were used to study the formation of the TR–CD complexes using a coprecipitation technique. The results showed that TR did not form a complex with αCD, whereas it forms complexes partially with βCD and completely with γCD. These findings are supported by FT-IR, differential scanning calorimetry, and X-ray diffraction analyses. The electrospun BPU/TR–CD nanofibers were investigated in terms of morphology, releasing behavior, and antibacterial tests. The BPU/TR–γCD nanofiber shows better antibacterial activity than the others. The results obtained in this study are expected to broaden the range of biobased polyurethane applications where antibacterial properties are required.

1. Introduction

Cyclodextrins (CDs) are nontoxic cyclic oligosaccharides and are classified according to their number of glucopyranose units.[1] The most-used CDs include αCD (cyclohexaamylose, six units of glucopyranose), βCD (cycloheptaamylose, seven units of glucopyranose), and γCD (cyclooctaamylose, eight units of glucopyranose). They are nontoxic, biocompatible, inexpensive, and produced naturally by enzymatic degradation of starch.[2–4] Moreover, they have a unique cone-shaped molecular structure which leads to the special ability to form complexes with various guest materials, such as drugs, antibacterial agents, and food additives.[5,6] Moreover, the CD complexes can improve the stability, solubility, bioavailability, and releasing properties of the guest molecules.[7–9]

Triclosan (TR) is a commonly used US Food and Drug Administration-approved synthetic nonionic broad-spectrum antimicrobial agent used in consumer or medical products including toothpastes, soap, detergents, and surgical cleaning treatments.[10,11] However, TR is a hydrophobic and poorly water soluble drug. Because its antibacterial properties can be improved by increasing its solubility in water, TR–CD complexes have been widely researched as antimicrobial agents.[12,13]

Polyurethane (PU) is the most widely used polymer for various applications, such as coatings, adhesives, sealants, foams, and composites.[14–17] PU is mainly synthesized using a polyaddition reaction with multiple hydroxyl groups and two or more isocyanate groups. To meet the growing demand for sustainability of resources, it is desirable to develop a bio-polyurethane (BPU) as a next-generation elastomer from renewable raw materials and these BPUs are expected to replace the petroleum-based PU in high-value-added industries such as bioelastomers, stretchable nanofilters with long-term durability, wound dressing, and drug-delivery materials.[18–20] Bio-based polyols are commonly used to produce BPU because the range of commercially available isocyanates is limited. Among the sustainable biobased materials, plant oils have attracted much attention as sustainable polyols for preparing BPU. Plant oils are triglycerides containing three saturated or unsaturated fatty acids. Castor oil (CO) can be used as a polyol without further functionalization because it has inherent hydroxyl groups. In one of our previous research, the CO/polycaprolactone diol (PCL-diol) hybrid polyol based BPUs were produced. The hybridization of PCL-diol with CO provided outstanding shape memory properties, including both shape retention and shape recovery, of the BPU synthesized therefrom. Moreover, the BPU showed faster enzymatic degradation that conventional petroleum based polyurethane.[21]

[a]*Department of Organic and Nano Engineering, College of Engineering, Hanyang University, Seoul, Korea. E-mail: kimsh@hanyang.ac.kr; Fax: +82-2-2281-2737; Tel: +82-2-2220-0496*

[b]*LG Hausys R&D Center, Seoul, Korea*

† Both authors contributed equally to this work.

PU nanofibers made using the electrospinning technique have been continuously studied because of their potential for bioengineering and medical applications.[22–24] Electrospinning is the most common, efficient, and inexpensive method to produce a continuous nanofiber web using polymeric materials. The electrospun nanofibers have a small diameter, a large surface area per unit mass, flexure, and there are many microspaces between the fibers. Therefore, it is possible to widen the biomedical application fields by incorporating other materials in electrospun nanofibers. Several researchers have reported the fabrication of composite nanofibers containing nanocellulose,[25] silver nanoparticles (AgNPs),[26] AgNPs anchored TiO$_2$,[27] Pd,[28] and salicylic acid[29] for application of antibacterial, photocatalyst, and biomedical applications.

Herein, BPU nanofibers containing TR–CD complexes (BPU/TR–CD) to enhance antibacterial properties were prepared using an electrospinning method. The BPU was successfully synthesized using castor oil or castor oil/poly(caprolactone)diol (PCL-diol) hybrid polyol. The chemical structure and mechanical properties of the BPU were characterized using Fourier transform infrared (FT-IR), proton nuclear magnetic resonance (^{1}H-NMR), and a universal testing machine (UTM). The TR–CD complexes were prepared using a coprecipitation method of TR and αCD, βCD, and γCD. The obtained TR–CD complexes were investigated using FT-IR, differential scanning calorimetry (DSC), and X-ray diffraction (XRD). The BPU/TR–CD nanofibers were analyzed in terms of their morphology, releasing behavior, and antibacterial efficiency.
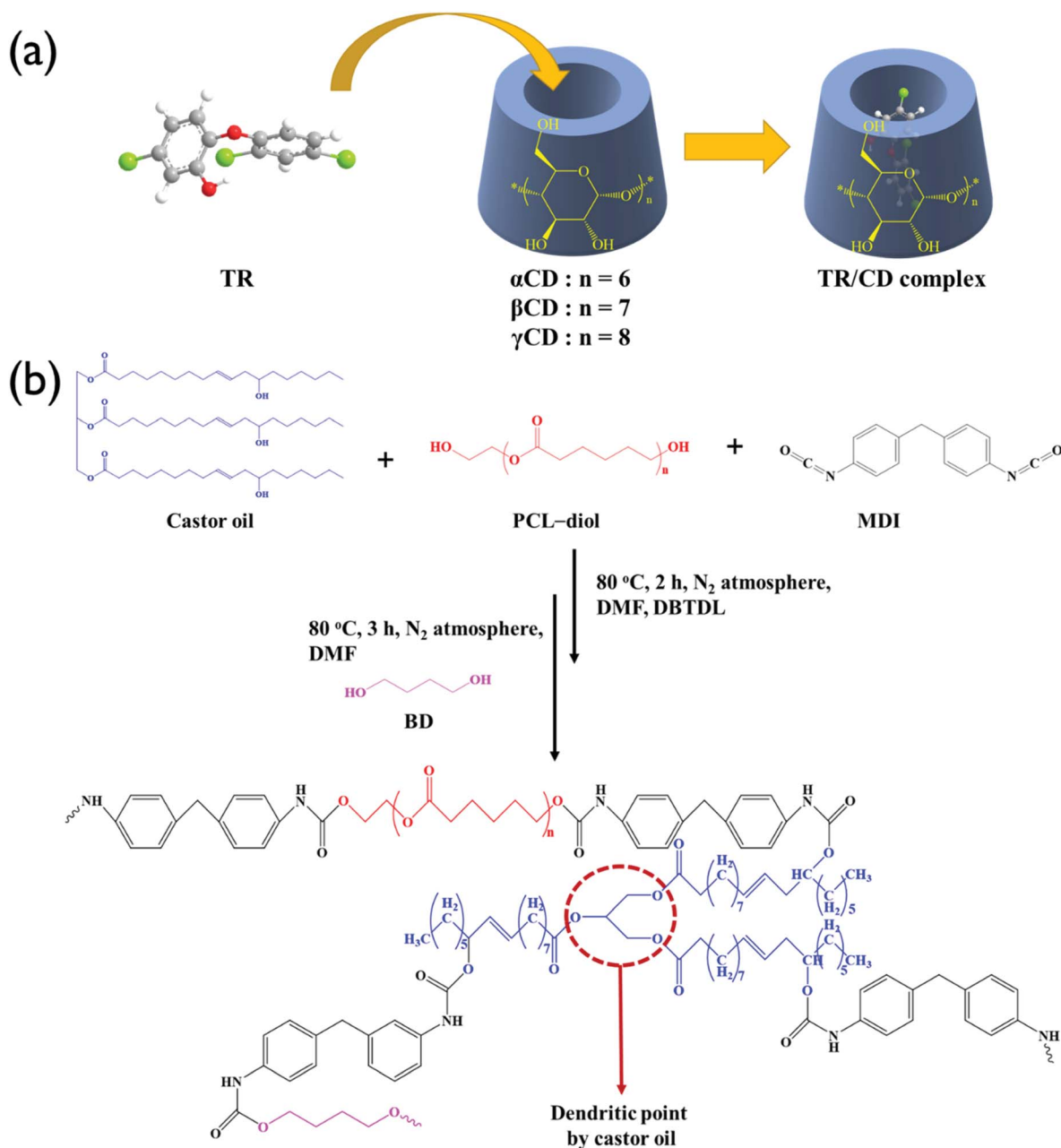

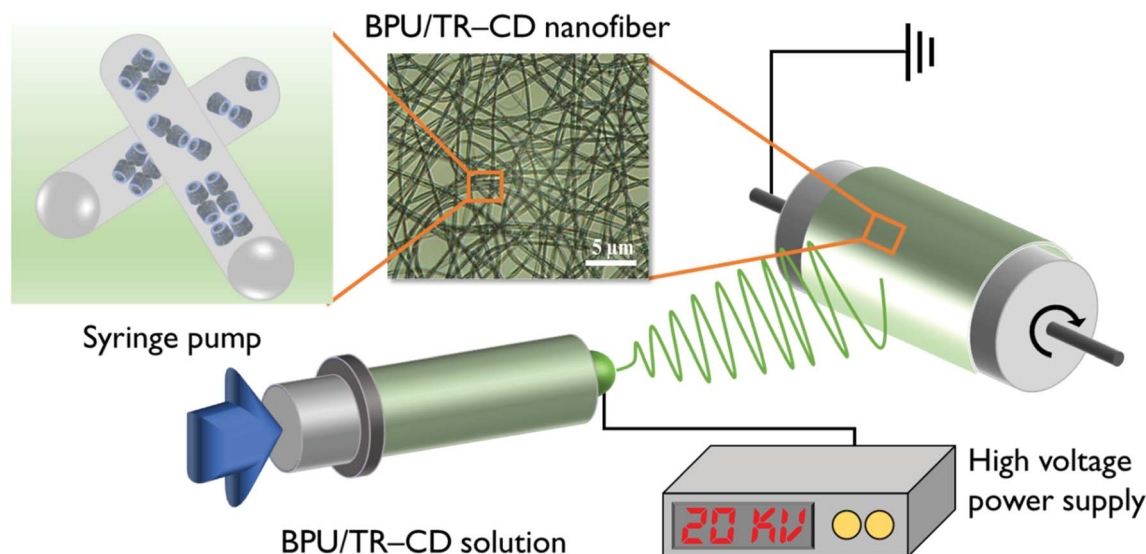**Fig. 1** Formation of the TR–CD complexes (a) and synthesis pathway of the BPU (b).

BPU/TR–CD nanofiber

Syringe pump

BPU/TR–CD solution

High voltage power supply

20 KV

5 μm

Fig. 2 Electrospinning of BPU/TR–CD complexes.

2. Experimental

2.1. Materials

Castor oil, PCL-diol (molar mass = 2000 g mol^{-1}), methylenediphenyl diisocyanate (MDI), dibutyltindilaurate (DBTDL), and TR were purchased from Sigma Aldrich (Seoul, Korea). 1,4-Butanediol (BD) was obtained from Junsei Chemical (Tokyo, Japan). αCD, βCD, and γCD were purchased from Tokyo Chemical Industry (Tokyo, Japan), and dimethylformamide (DMF) was supplied by Duksan, Korea. All reagents were used as received without further purification.

2.2. Preparation of TR–CD complexes

TR–CD complexes were prepared using the coprecipitation method as shown in Fig. 1(a). For all samples, the molar ratio of TR to CD was 1 : 1. Three 0.16 g (5.52 × 10^{-4} mol) samples of TRs were stirred in 2 mL of water for 1 h. Then, 0.54 g of αCD, 0.63 g of βCD, and 0.72 g of γCD were dissolved in 3.7 mL, 33.9 mL, and 3.1 mL of water at room temperature, respectively. Each concentration was determined by the solubility in water at 25 °C; 14.5 g/100 mL for αCD, 1.85 g/100 mL for βCD, and 23.2 g/100 mL for γCD. The aqueous CD solutions were added to the aqueous TR suspension dropwise, followed by mixing at 60 °C for 1 h. Then, the solutions were cooled to room temperature and stirred gently for 24 h. In the case of TR–αCD, the TR particles settled, indicating that the complex was not well formed. The obtained TR–βCD and TR–γCD suspensions were filtered and washed repeatedly with water. Finally, vacuum-dried white TR–βCD and TR–γCD powders were collected.

2.3. Synthesis of BPU

The BPU used in this study was prepared according to the method reported in our previous research.[21,25] The synthesis scheme is shown in Fig. 1(b). The reaction was carried out in two steps; the first step is the synthesis of PU prepolymer and the second step is chain extension with BD. Briefly, the castor oil/PCL-diol hybrid polyol in a molar ratio of 1 : 9 was mixed under gentle stirring at 50 °C for 30 min, followed by reaction with MDI dissolved in DMF at 80 °C for a period of 2 h. Then, the BD in DMF was added dropwise and stirred for another 3 h. DBTDL (0.03 wt% to PU) was used as catalyst and all reactions were carried out under a nitrogen atmosphere. The amount of reactant was determined according to the NCO : OH ratio of 1. Finally, the solution was cast onto a PTFE mold and the solvent was allowed to evaporate at 80 °C overnight. The obtained PU was stabilized at room temperature for 1 week.

2.4. Electrospinning of BPU/TR–CD nanofibers

BPU/TR–CD nanofibers were produced using an electrospinning machine with a high-voltage power supply (ESP200D; NanoNC, Seoul, Korea) as shown in Fig. 2. To prepare the BPU/TR–CD nanofibers, the desired amounts of TR–βCD and TR–γCD were dispersed in the BPU/DMF solutions. The solutions were stirred, followed by further ultrasonication for 10 h to obtain a good dispersion. The composition and viscosity of the electrospinning solutions are summarized in Table 1. A voltage of 20 kV was applied to the collecting target using a high-voltage power supply, and the flow rate for the solution was 1 mL h^{-1}.

Table 1 The composition and viscosity of the solutions used for electrospinning

Solutions	% BPU[a] (w/v)	% TR–CD[b] (w/w)	% TR (w/w)	Viscosity (Pa s)
BPU	30		—	0.13
BPU/TR	30		4	0.14
BPU/TR–βCD	30	16.7	—	—
BPU/TR–γCD	30	20	—	0.16

[a] With respect to solvent. [b] With respect to the BPU.

The inner diameter of the spinneret was 0.8 mm. The electrospun nanofibers were collected on a rotary target drum, which was placed at a distance of 15 cm from the needle tip. This process was selected as the optimal process to obtain well-electrospun nanofibers.

2.5. Characterization

FT-IR spectroscopy (PerkinElmer Spectrum 2000) equipped with a single-reflection attenuated total reflectance system (Specac, London, UK) was used to determine the chemical structure of the BPU and TR–CD complexes. The further analysis of the BPU structure was carried out using a proton nuclear magnetic resonance (^{1}H-NMR; Bruker D PX-400) system. The mechanical property of the BPU was measured using a UTM (Instron 4465) equipped with standard fiber grips. The field-emission scanning electron microscope (JSM-6340F; JEOL, Hitachi, Japan) was used to analyze the morphology of the BPU/TR–CD nanofibers. The distribution of diameters for the nanofibers was determined using image analysis software (Image-Pro Plus; Media Cybernetics, Rockville, MD, USA). Thermogravimetric analysis (TGA) was carried out using a Pyris 1 TGA (PerkinElmer, Waltham, MA, USA) under a nitrogen atmosphere at a heating rate of 10 °C min^{-1}. Fourier transform infrared spectroscopy (FT-IR, Nicolet 760 MAGNa-IR spectrometer) was used to determine the structure of the TR, CDs, and TR–CDs over the range of 500–4000 cm^{-1}. ^{1}H-NMR (Varian VNMRS 600 MHz spectrometer) and C-NMR was used to further structural analysis for the TR–CDs. The thermal behavior of the TR–CDs was measured using a PerkinElmer DSC7 over the temperature range 30–200 °C at a scan rate of 10 °C min^{-1}. For crystallinity analysis of TR–CDs, XRD patterns were determined using X-ray diffractometry (Rigaku Denki, Tokyo, Japan) at 40 kV and 60 mA and the XRD was scanned in a 2θ range of 5–45°. Controlled release measurements were performed with square pieces of BPU/TR and BPU/TR–CD nanofibers which were added to phosphate buffer saline (PBS) (pH 7.4) and incubated at 37 °C in an orbital shaker at 200 rpm. Drug concentration was determined using UV spectroscopy and the calibration curves were obtained plotting absorbance at 281 nm, the absorbance peak

of triclosan. Samples were withdrawn at certain time intervals. Antibacterial activity tests were carried out according to the KS K 0693-2006 method to detect bacteriostatic activity on fiber mats. The antibacterial properties of BPU/TR–CD nanofibers were investigated against *Staphylococcus aureus* (Gram-positive bacterium, ATCC 6538) and *Klebsiella pneumonia* (Gram-negative bacterium, ATCC 4532). The cytostatic efficiency (%) was calculated as follows:

$$\text{Cytostatic efficiency } (\%) = \frac{M_b - M_c}{M_b} \times 100,$$

where M_a is the initial average number of bacteria (CFU: colony-forming unit) and M_b is the average number of bacteria (CFU) after incubation for 18 h. M_c is the average number of bacteria (CFU) after the cytostatic test.

3. Result and discussion

3.1. Preparation of TR–CD complexes

The TR–CD complexes were prepared using three types of CDs (αCD, βCD, and γCD) to enhance the solubility and antibacterial activity of TR. Referring to other literature, the diameter of the CD cavity is in the order γCD (0.95 nm) > βCD (0.78 nm) > αCD (0.57 nm) with the same cavity depth (≈ 8 Å). The αCD, whose cavity size is small, could not form the TR–CD complex, so αCD was not a suitable host for TR. The chemical structures of the TR–CDs and pure TR, as well as the pure CD, are shown in Fig. 3(a). The transmittance peaks for the pure CD (βCD and γCD) detected at around 1030, 1080, and 1157 cm^{-1} are related to the coupled C–C/C–O stretching vibrations and the C–O–C glycosidic bridge asymmetric stretching, respectively. The pure TR showed three characteristic peaks around 1418, 1472, and 1505 cm^{-1}, which were assigned to the skeletal vibrations of C–C stretching in the benzene ring. In the TR–βCD and TR–γCD samples, both the aforementioned TR and CD characteristic peaks were displayed, suggesting the successful preparation of the TR–CD complex. The ^{1}H-NMR spectrum of the TR–γCD complex is shown in Fig. 3(b). Prior to structural analysis of the complex, a ^{1}H-NMR analysis was carried out in order to identify the characteristic peaks corresponding to their protons. It was
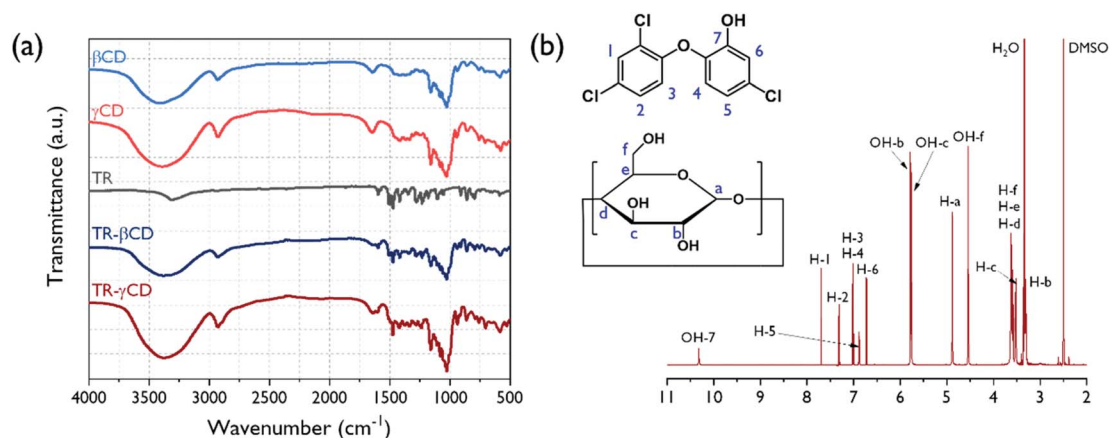

Fig. 3 FT-IR spectra of pure βCD, γCD, TR, and TR–CD complexes (a) and ^{1}H-NMR spectra of TR–γCD complex dissolved in DMSO-d_6 (b).

observed that the peaks for TR and CD were not overlapped (data not shown). The peaks of TR were observed in the region of 6.6–10.3 ppm, and peaks of the γCD were observed in the region of 3.1–5.9 ppm.

The TR–βCD and TR–γCD complexes were further characterized using DSC by which the formation of the host–guest complex was verified. As shown in Fig. 4(a), strong endothermic peaks around 59 °C are observed in both TR and TR–αCD, implying that the formation of the TR–αCD complex was unsuccessful. However, the small melting peak around 57 °C detected in the TR–βCD complex indicates the presence of some uncomplexed TR crystals. However, in the case of the TR–γCD complex, the melting peak for free TR was not observed, which demonstrates the TR was fully complexed with the γCD.

To investigate the crystalline structures of the TR, TR–βCD, and TR–γCD, XRD analysis was carried out and the results are shown in Fig. 4(b). TR shows sharp peaks at $2\theta = 8.0, 14.0, 16.2, 21.5, 24.3, 25.3$, and $29.4°$; therefore, it is confirmed that the TR is a crystalline material. According to Jug et al., the crystal structure of the TR is maintained even after high-vibration micromilling for about 80 min.[30] Thus, the crystal peak of TR can provide important information for understanding the structure of the TR–CD complexes. The βCD or γCD can be classified by two crystal structures into "cage" and "channel"

types. The cage types exist only when the water molecule is a guest, whereas the channel type can be formed when other guest molecules are present, including both small and macromolecules. Therefore, identifying the channel-type crystal structures for the CDs is a measure of whether the complex is well formed.[31] In the case of TR–βCD, the presence of peaks at $2\theta = 12.1$ and $17.8°$ shows formation of a channel-type βCD. However, a peak at $2\theta = 8.0°$ also appeared, which corresponds to the crystal peak of the TR, indicating that there is some uncomplexed TR in the complex. This result supports the DSC analysis described above. For the TR–γCD, typical crystal peaks of a channel-type γCD, which correspond to $2\theta = 7.4, 14.2, 14.9, 15.8, 16.6$, and $21.8°$, were shown. Moreover, no sign was found of uncomplexed TR. It is confirmed once again that the γCD formed a complete complex with the TR.

The thermal degradation behavior of the TR–γCD and its precursors were analyzed by TGA (Fig. 5(a)). Thermal decomposition of TR did not occur until the temperature reached 170 °C, which means that oxidation did not occur. In case of the γCD and TR–γCD, the TGA thermograms show weight losses below 100 °C due to evaporation of water molecules. As shown in Fig. 5(b), the TR–γCD shows two thermal degradation steps. At the first step between 210 °C and 340 °C, the degradation of
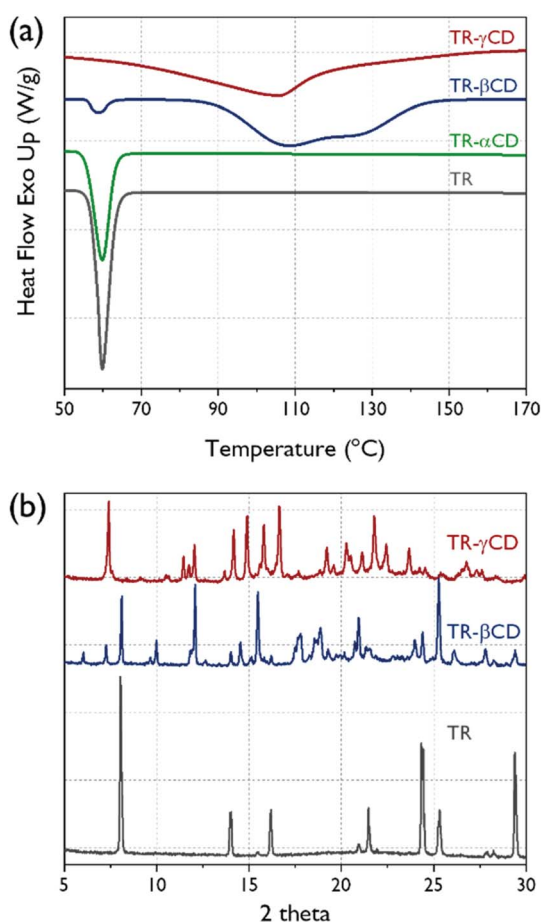

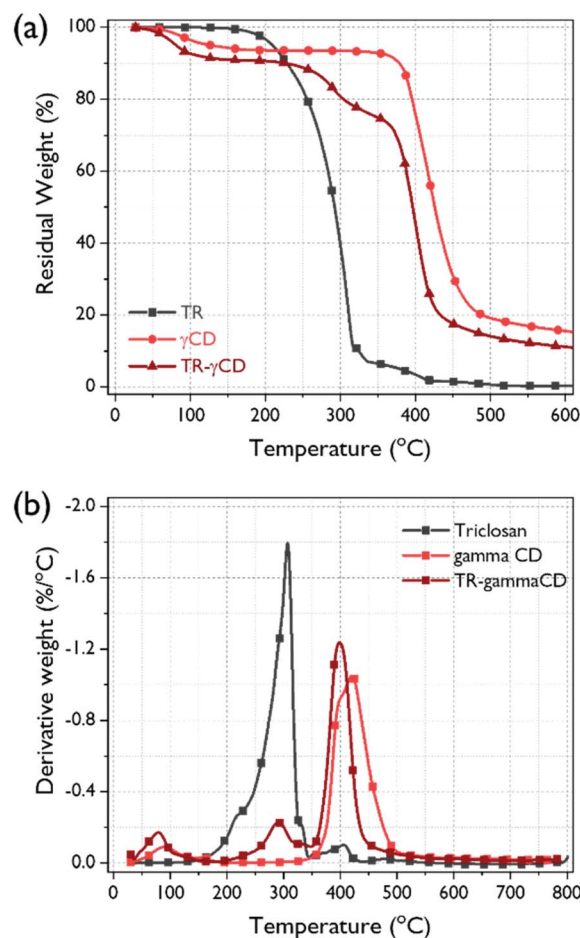Fig. 4 (a) DSC thermograms of pure TR and TR−CD complexes, (b) XRD patterns for pure TR and the TR−CD complexes.

Fig. 5 (a) TGA thermograms of TGA thermograms of TR, γCD, and TR−γCD complex, and (b) their derivatives.

free TR starts. This decomposition temperature is consistent with that of TR. At the second step between 340 °C and 520 °C is due to the complete degradation of the complex. These thermal degradation behaviors of the cyclodextrin complex are also reported in previous studies.[32,33] The relative reduction in amount of thermal degradation for the free TR and the increase in degradation temperature of the TR–CD complex can further support the successful formation of the complex.

3.2. Preparation of BPU nanofiber

Several studies have been reported using castor oil as a cross-linker for hyperbranched PU.[34,35] In general, PU with high crosslinking density has a drawback limiting application fields, such as electrospinning and coating solution, because of its insolubility in common organic solvents. To overcome this shortcoming, we have tried to prepare PU with hybrid polyol mixed with castor oil and PCL-diol. The possible structure of the BPU is presented in Fig. 1(b). The castor oil in hybrid polyols was employed as dendritic points due to its characteristic triglyceride groups. The PCL-diol, which is a major component of the hybrid polyol, makes it possible to dissolve BPU in organic solvents by forming a linear structure. Therefore, electrospinning was possible using a solution of BPU dissolved in DMF. To determine the chemical structure of the electrospun BPU, FT-IR analysis was carried out. As shown in Fig. 6(a), the disappearance of the distinctive peak corresponding to the isocyanate group around 2270 cm^{-1} in BPU indicates that the polymerization was successful. The two bands observed around 3324 cm^{-1} and 1731 cm^{-1} can be assigned to the N–H stretching and C=O stretching, respectively, which clearly support the successful synthesis of PU. Another peak at 1533 cm^{-1} is detected due to the N–H bending vibration of the urethane linkage, and the bands in the region of 3000–2800 cm^{-1} correspond to the symmetric and asymmetric stretching vibrations of the aliphatic CH$_2$ and CH$_3$ groups.[36] Further analysis of the BPU structure using ^{1}H-NMR spectroscopy was carried out (Fig. 6(b)). The degree of branching (DB) of branched BPUs was determined using Frechet's equation[37] as follows:

$$DB = (D + T)/(D + T + L),$$

where D, T, and L are the numbers of dendritic units, terminal units, and linear units, respectively, in the branched structure.[38] In general, DB is evaluated from NMR spectroscopy by comparing the integration of the peaks for the respective units. However, the dendritic, terminal, and linear units were not easily distinguished due to the complex structure of triglyceride ricinoleic acids in castor oil. Therefore, the reacted and unreacted OH functional groups were used to determine DB. The relative amounts of the reacted and unreacted units were calculated by the integration of the ^{1}H-NMR peaks of secondary C–H of substituted OH to urethane [O–(C=O)–NH] ($\delta = 3.91$–4.15) and unsubstituted OH ($\delta = 3.71$–3.88). The calculated DB value is 0.38 from the integration of the ^{1}H-NMR peaks. This value indicated that the synthesized BPU exhibited a branched structure. In general, a dendrimer has a DB value of close to unity and a hyperbranched polymer has a DB value close to 0.5 while the DB value of a linear structure is closer to zero.[38] The mechanical properties of electrospun BPU were investigated using a tensile test, and the stress–strain curves are shown in Fig. 6(c). From the result, the elongation at break, tensile strength, and Young's modulus are summarized in the inset table in that figure. The profiles of the stress–strain curves mean that the BPU is a typical elastomer in the form of dispersed hard domain in a soft domain matrix. The electrospun BPU exhibited high flexibility and elastic property with a high ductile elongation at break of 219.7% and a tensile strength of 2.3 MPa. Therefore, the electrospun BPU is suitable for encapsulating the TR–CD complexes and expected to be useful in various application fields.

3.3. Morphology of BPU/TR nanofibers

The introduction of TR–CD complexes in BPU nanofibers was achieved by an electrospinning process of the solution mixture of BPU and TR–CD complexes. For comparison, BPU/TR nanofiber was also prepared under the same conditions. The SEM images and diameter distributions of the obtained nanofibers are shown in Fig. 7. The BPU and BPU/TR nanofibers show a uniform distribution in fiber diameter smooth surface, and bead-free morphology. The average fiber diameter was 237.4 nm. On the other hand, the BPU/TR–CD nanofibers displayed a relatively irregular distribution in fiber diameter, though it still showed a bead-free morphology. This is attributed to their heterogeneous system and the aggregates of TR–CD crystals. In our previous research, we confirmed the heterogeneity of PU/modified silica dope solution from a decrease in the gradient of the rheological Cole–Cole plot, which causes an irregularity of the electrospun nanofiber diameter.[39] Because of their irregularity, thinner
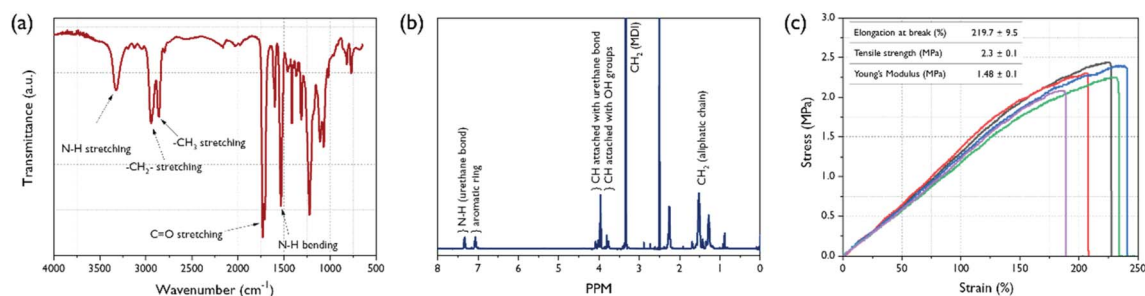
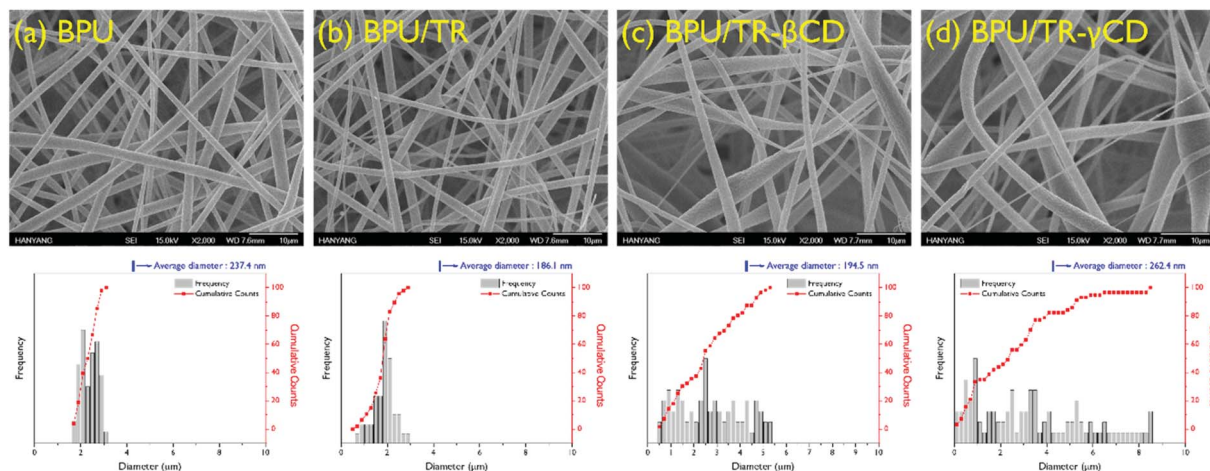**Fig. 6** FT-IR spectrum (a), ^{1}H-NMR spectrum (b) for the BPU, and stress–strain curves (c) for the BPU nanofiber.

Fig. 7 SEM images and fiber diameter distribution of (a) BPU, (b) BPU/TR, (c) BPU/TR–βCD, and (d) BPU/TR–γCD nanofibers.

nanofibers may also be observed than the neat BPU, resulting in lower average diameter of nanofibers of BPU/TR and BPU/TR–βCD. Jung *et al.* also reported a similar phenomenon in silica/polyacrylonitrile nanofiber.[40] As the TR–CD complexes were added, it was observed that the nanofiber surface became rougher.

3.4. *In vitro* release study

Fig. 8 presents the releasing behavior of BPU hybrid nanofibers when they were exposed to a hydrophilic phosphate buffer. The TR or TR–CD complexes loaded in BPU nanofiber do not deform and maintain their structures because the peak position of the maximum absorbance of TR was not changed. The increase in UV absorbance of TR means an increase in concentration of released TR and the encapsulation of TR or TR–CD complexes into the BPU nanofibers. After rapid initial release, the release of TR reached steady state for BPU/TR and BPU/TR–βCD. These results have been reported by earlier studies dealing with water insoluble drug/cyclodextrin complexes.[41,42] For the BPU/TR, the

saturated concentration of antibacterial agent is significantly lower than those of BPU/TR–CD complexes, which is mainly dependent on the affinity between the guest material and the release medium. TR is practically insoluble in PBS as demonstrated elsewhere.[33] Incorporation of TR as complex with βCD and γCD significantly enhanced their *in vitro* drug release rates. The release profiles reached 92.1% and 82.3% for the BPU/TR–γCD and BPU/TR–βCD, respectively. This is because the solubility of the TR–CD complexes with released medium was remarkably improved.[43–45] This indicates the efficient drug-releasing properties of the BPU/TR–CD nanofibers in aqueous system. This result can be supported by the DSC and XRD patterns described above, the more that TR forms a complex with CD, the more releases occur in an aqueous system.

3.5. Antibacterial activity

Antibacterial tests for neat BPU, BPU/TR, BPU/TR–βCD, and BPU/TR–γCD nanofibers were conducted using representative Gram-positive (*S. aureus*) and -negative (*K. pneumonia*) bacteria. *S. aureus* is a virulent pathogen which is the main cause of skin infections, respiratory infections such as sinusitis, and food poisoning. *K. pneumonia* causes bacterial pneumonia and is commonly implicated in wound infections, particularly of immunocompromised individuals. Table 2 summarizes the cytostatic activity and efficiency of the neat BPU and BPU/TR, BPU/TR–CD complexes nanofibers according to bacteria kinds, and the images are shown in Fig. 9. The calculated cytostatic efficiency of the neat BPU nanofibers is 43.7% and 73.5% against *S. aureus* and *K. pneumonia*, respectively. These values are lower than that for cotton, implying that the neat BPU nanofibers have no cytostatic ability. On the other hand, the cytostatic efficiency values of BPU/TR–βCD and BPU/TR–γCD nanofibers were higher than 99.9% for both Gram-positive and -negative bacteria, when the BPU/TR nanofibers showed cytostatic efficiency values of 97.0% and 98.1% against *S. aureus* and *K. pneumonia*, respectively. From this result, it is remarkable that the TR–CD complexes in the BPU nanofibers played a crucial role to keep down bacterial viability with excellent
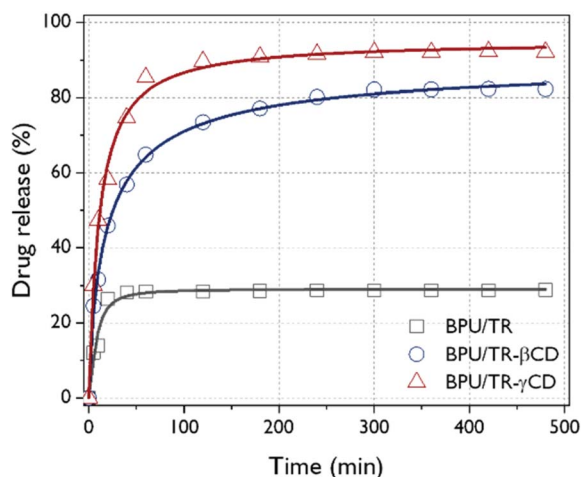

Fig. 8 Release curves of BPU/TR and BPU/TR–CD nanofibers in phosphate buffer saline medium.

Table 2 Antibacterial ability of the neat BPU, BPU/TR, and BPU/TR−CD nanofibers according to bacteria strains

Sample	BPU		BPU/TR		BPU/TR−βCD		BPU/TR−γCD	
Bacteria type	S. aureus (ATCC 6538)	K. pneumonia (ATCC 4352)	S. aureus (ATCC 6538)	K. pneumonia (ATCC 4352)	S. aureus (ATCC 6538)	K. pneumonia (ATCC 4352)	S. aureus (ATCC 6538)	K. pneumonia (ATCC 4352)
M_a^a (CFU^d)	1.2×10^5	1.1×10^5	1.2×10^5	1.1×10^5	1.2×10^5	1.1×10^5	1.2×10^5	1.1×10^5
M_b^b (CFU)	6.8×10^6	5.7×10^6	6.8×10^6	5.7×10^6	6.8×10^6	5.7×10^6	6.8×10^6	5.7×10^6
M_c^c (CFU)	3.8×10^6	1.5×10^6	2.0×10^5	1.1×10^5	<10	<10	<10	<10
Cytostatic activity^e	0.2	0.6	1.5	1.7	>5.8	>5.8	>5.8	>5.8
Cytostatic efficiency^f (%)	43.7	73.5	97.0	98.1	99.9	99.9	99.9	99.9

^{a} M_a: initial average number of bacteria. ^{b} M_b: average number of bacteria after bacterial culture for 18 h. ^{c} M_c: average number of bacteria after the antibacterial test. ^{d} CFU: colony-forming unit. ^{e} Cytostatic activity: $\log M_b - \log M_c$. ^{f} Cytostatic efficiency (%): $[(M_b - M_c)/M_b] \times 100$.
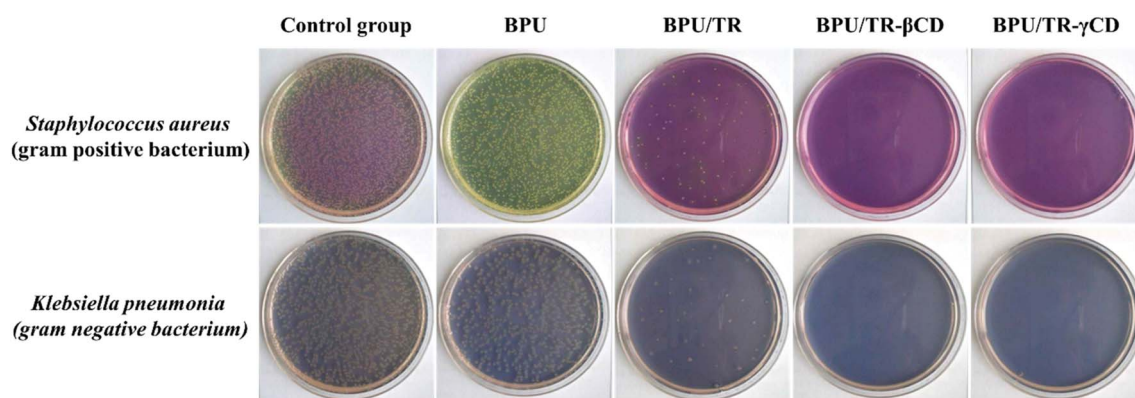

Fig. 9 The images of antibacterial test according to bacterium strains.

antibacterial ability because of their improved solubility and releasing properties in aqueous medium.[46]

4. Conclusion

Herein, electrospun BPU nanofibers were successfully embedded with TR–CD complexes to prepare antibacterial nanofibers. The BPU was synthesized using PCL-diol and castor oil hybrid polyol, and its structure was evaluated using FT-IR and ¹H-NMR analysis. TR did not form a complex with αCD, however, it forms complexes partially with βCD and completely with γCD, which is supported by FT-IR, DSC, and XRD analyses. The electrospun BPU/TR–CD nanofibers were characterized in terms of morphology, drug release behavior, and antibacterial test. The BPU/TR–γCD nanofiber has shown better antibacterial activity against S. aureus and K. pneumonia than the BPU, BPU/TR, and BPU/TR–βCD because of its enhancement in solubility of TR, which resulted in excellent release of the antibacterial agent from the nanofiber. Overall, it is considered that BPU/TR–CD nanofiber may find a wide range of applications where antibacterial properties are required.

Conflicts of interest

There are no conflicts to declare.

Acknowledgements

References

1 A. R. Hedges, Chem. Rev., 1998, 98, 2035–2044.
2 S. Davoodi, E. Oliaei, S. M. Davachi, I. Hejazi, J. Seyfi, B. S. Heidari and H. Ebrahimi, RSC Adv., 2016, 6, 39870–39882.
3 A. Alsbaiee, B. J. Smith, L. Xiao, Y. Ling, D. E. Helbling and W. R. Dichtel, Nature, 2016, 529, 190.
4 Z. I. Yildiz, A. Celebioglu, M. E. Kilic, E. Durgun and T. Uyar, J. Food Eng., 2018, 224, 27–36.
5 I.-K. Park, H. A. Von Recum, S. Jiang and S. H. Pun, Langmuir, 2006, 22, 8478–8484.
6 J. Wang, Y. Cao, B. Sun and C. Wang, Food Chem., 2011, 127, 1680–1685.
7 T. Loftsson and D. Duchene, Int. J. Pharm., 2007, 329, 1–11.
8 Z. Aytac, S. I. Kusku, E. Durgun and T. Uyar, Mater. Sci. Eng. C, 2016, 63, 231–239.

9 M. Jug, F. Maestrelli and P. Mura, *J. Incl. Phenom. Macrocycl. Chem.*, 2012, **74**, 87–97.

10 T. Yorozu, M. Hoshino, M. Imamura and H. Shizuka, *J. Phys. Chem. A*, 1982, **86**, 4422–4426.

11 M. Jug, I. Kosalec, F. Maestrelli and P. Mura, *Carbohydr. Polym.*, 2012, **90**, 1794–1803.

12 F. Kayaci, O. C. Umu, T. Tekinay and T. Uyar, *J. Agric. Food Chem.*, 2013, **61**, 3901–3908.

13 H. Ogihara, J. Xie, J. Okagaki and T. Saji, *Langmuir*, 2012, **28**, 4605–4608.

14 C. K. Park, J. H. Lee, I. S. Kim and S. H. Kim, *J. Appl. Polym. Sci.*, 2019, 48304.

15 H. Du, Y. Zhao, Q. Li, J. Wang, M. Kang, X. Wang and H. Xiang, *J. Appl. Polym. Sci.*, 2008, **110**, 1396–1402.

16 C. Wang, Y. Wu, Y. Li, Q. Shao, X. Yan, C. Han, Z. Wang, Z. Liu and Z. Guo, *Polym. Adv. Technol.*, 2018, **29**, 668–676.

17 S. Thakur and N. Karak, *ACS Sustain. Chem. Eng.*, 2014, **2**, 1195–1202.

18 S. Thakur and N. Karak, *New J. Chem.*, 2015, **39**, 2146–2154.

19 R. Bayan and N. Karak, *Composites, Part A*, 2018, **110**, 142–153.

20 J. Y. Cherng, T. Y. Hou, M. F. Shih, H. Talsma and W. E. Hennink, *Int. J. Pharm.*, 2013, **450**, 145–162.

21 K. K. Choi, S. H. Park, K. W. Oh and S. H. Kim, *Macromol. Res.*, 2015, **23**, 333–340.

22 K. Kim, Y. K. Luu, C. Chang, D. Fang, B. S. Hsiao, B. Chu and M. Hadjiargyrou, *J. Control. Release*, 2004, **98**, 47–56.

23 H. Nie, J. Li, A. He, S. Xu, Q. Jiang and C. C. Han, *Biomacromolecules*, 2010, **11**, 2190–2194.

24 M. A. Alvarez-Perez, V. Guarino, V. Cirillo and L. Ambrosio, *Biomacromolecules*, 2010, **11**, 2238–2246.

25 S. H. Park, K. W. Oh and S. H. Kim, *Compos. Sci. Technol.*, 2013, **86**, 82–88.

26 A. W. Jatoi, I. S. Kim and Q. Q. Ni, *Mater. Sci. Eng. C*, 2019, **98**, 1179–1195.

27 A. W. Jatoi, I. S. Kim and Q.-Q. Ni, *Carbohydr. Polym.*, 2019, **207**, 640–649.

28 H. Lee, M. Kim, D. Sohn, S. H. Kim, S.-G. Oh, S. S. Im and I. S. Kim, *RSC Adv.*, 2017, **7**, 6108–6113.

29 B. Pant, M. Park, G. P. Ojha, D.-U. Kim, H.-Y. Kim and S.-J. Park, *Int. J. Polym. Mater.*, 2018, **67**, 739–744.

30 M. Jug, I. Kosalec, F. Maestrelli and P. Mura, *J. Pharm. Biomed. Anal.*, 2011, **54**, 1030–1039.

31 M. H. Ja, N. Kamal, B. Y. Hui and M. Fahmi, *Sains Malays.*, 2018, **47**, 977–989.

32 M. F. Canbolat, A. Celebioglu and T. Uyar, *Colloids Surf., B*, 2014, **115**, 15–21.

33 M. Novikov, K. L. Thong, N. I. M. Zazali and S. B. A. Hamid, *Fibers Polym.*, 2018, **19**, 548–560.

34 S. Oprea, *J. Am. Oil Chem. Soc.*, 2010, **87**, 313–320.

35 S. Oprea, V. O. Potolinca, P. Gradinariu, A. Joga and V. Oprea, *Cellulose*, 2016, **23**, 2515–2526.

36 P. K. Behera, P. Mondal and N. K. Singha, *Polym. Chem.*, 2018, **9**, 4205–4217.

37 H. S. Lee, Y. K. Wang and S. L. Hsu, *Macromolecules*, 1987, **20**, 2089–2095.

38 Y. M. Boyarchuk, L. Y. Rappoport, V. Nikitin and N. Apukhtina, *Polym. Sci. U. S. S. R.*, 1965, **7**, 859–867.

39 S. H. Park, Y. S. Ryu and S. H. Kim, *J. Mater. Sci.*, 2015, **50**, 1760–1769.

40 H.-R. Jung, D.-H. Ju, W.-J. Lee, X. Zhang and R. Kotek, *Electrochim. Acta*, 2009, **54**, 3630–3637.

41 M. Mehrizi, S. Amiri, S. Hajir Bahrami and R. Mirzaee, *J. Text. Inst.*, 2019, 1–13.

42 X.-Z. Sun, G. R. Williams, X.-X. Hou and L.-M. Zhu, *Carbohydr. Polym.*, 2013, **94**, 147–153.

43 R. Zurita, J. Puiggalí and A. Rodríguez-Galán, *Macromol. Biosci.*, 2006, **6**, 58–69.

44 A.-H. Pei, Z.-W. Shen and G.-S. Yang, *Mater. Lett.*, 2007, **61**, 2757–2760.

45 Y. Gao, G. Li, Z. Zhou, L. Guo and X. Liu, *Colloids Surf., B*, 2017, **160**, 364–371.

46 Y. Su, L. Zhao, F. Meng, Z. Qiao, Y. Yao and J. Luo, *Mater. Sci. Eng. C*, 2018, **93**, 921–930.